The crystal structures and physical properties of the solid solution compound $Ba_5Y_{8-x}Mn_4O_{21-1.5x}$ $(x = 0, 1)$*

Gao Qing-Qing(高庆庆), Li Jing-Bo(李静波)†, Song Shi-Jia(宋士佳), Rao Guang-Hui(饶光辉), Luo Jun(骆 军), Liu GuangYao(刘广耀), and Liang Jing-Kui(梁敬魁)‡

Beijing National Laboratory for Condensed Matter Physics, Institute of Physics, Chinese Academy of Sciences, Beijing 100190, *China*

(Received 21 December 2011; revised manuscript received 9 February 2012)

New oxometallides with the formula $Ba_5Y_{8-x}Mn_4O_{21-1.5x}$ (x = 0, 1) are prepared through an atmosphere-controlled solid-state reaction. Two single-phase samples with Ba/Y/Mn atomic ratios 5/8/4 (Y8) and 5/7/4 (Y7) are obtained. The crystal structures and the physical properties of the compounds are investigated by X-ray powder diffraction, magnetization, conductivity, and dielectricity measurements. The $Ba_5Y_{8-x}Mn_4O_{21-1.5x}$ compound is demonstrated to be a Y-deficient solid solution. The solid solution compound $Ba_5Y_{8-x}Mn_4O_{21-1.5x}$ crystallizes into tetragonal symmetry with the space group $I4/m$. Detailed structure analysis by Rietveld refinement of the X-ray powder diffraction data reveals that the Y vacancies occur preferentially at the Y(2) site. Thermal magnetization measurements indicate the presence of antiferromagnetic interaction between Mn ions in the compounds, and temperature-dependent resistivity measurements show that insulator–semiconductor transitions occur around 175 K and 170 K for the Y8 and Y7 samples, respectively. Strong frequency dependences of the dielectric constant are observed above ∼175 K for the two compounds.

Keywords: $Ba_5Y_{8-x}Mn_4O_{21-1.5x}$, X-ray powder diffraction, crystal structure, conductivity

PACS: 61.05.cp, 91.60.Ed, 72.20.–i **DOI:** 10.1088/1674-1056/21/6/066102

1. Introduction

Manganates have attracted extensive attention due to their promising physical properties, such as colossal magnetoresistance (CMR)[1,2] and magnetoelectric effects.[3] In order to search for novel rare-earth manganese oxides which may be potential candidates with promising physical properties, we studied the Y–Ba–Mn–O-based systems. New compounds, $Ba_5Y_{8-x}Mn_4O_{21-1.5x}$, belonging to the $Ba_5RE_8Mn_4O_{21}$-type oxometallate were obtained. The existence of $Ba_5RE_8Mn_4O_{21}$ compounds, each of which crystallizes into tetragonal symmetry with space group $I4/m$, was reported for RE = Nd,[4] Gd,[5] Sm, and Ho.[6] However, the relevant physical properties have been rarely reported in the literature. In the present work, the crystal structures and physical properties of the new compound, $Ba_5Y_{8-x}Mn_4O_{21-1.5x}$, are investigated by X-ray powder diffraction, magnetization measurements, and temperature-dependent resistivity and dielectric measurements. Changes in the structural parameters and physical properties of $Ba_5Y_{8-x}Mn_4O_{21-1.5x}$ induced by the Y-deficiency are discussed. To some extent, these investigations lead us to a comparative in-depth understanding of the intimate correlation between the physical properties and basic structures of the compounds.

2. Experiment

The compounds with atomic ratios of Ba:Y:Mn 5:8:4 and 5:7:4 (i.e. $Ba_5Y_8Mn_4O_{21}$ and $Ba_5Y_7Mn_4O_{19.5}$, denoted as Y8 and Y7, respectively, in this paper) were synthetized by the atmosphere-controlled solid-state reaction technique with precursors Y_2O_3, MnO_2, and $BaCO_3$ (purity > 99.9%). The powders of the precursors were stoichiometrically mixed and ground thoroughly. The mixtures were precalcined at 950 °C for 7 h, and then pressed into pellets. As is known, the valence state of Mn

*Project supported by the National Natural Science Foundation of China (Grant Nos. 50872148 and 51072225) and the National Basic Research Program of China (Grant No. 2007CB925003).

†Corresponding author. E-mail: jbli@iphy.ac.cn

‡Corresponding author. E-mail: jkliang@iphy.ac.cn

© 2012 Chinese Physical Society and IOP Publishing Ltd

is very sensitive to oxygen partial pressure, so the synthesis must be performed in a proper low oxygen partial pressure atmosphere. In our synthesis process, several Mn-containing oxides, $Ba_5Y_8Mn_4O_{21}$, MnO, $BaYMn_2O_5$, and $YMnO_3$, were produced while changing the oxygen partial pressure by passing a high-purity Ar flow over spongy titanium heated at slightly different temperatures. The oxygen partial pressure which determines the stability of the oxides has the following sequence for the oxides: $Mn^{2+}O \leq Ba_5Y_{8-x}Mn_4O_{21-1.5x} < BaYMn_2O_5 < YMnO_3$. We finally obtained the $Ba_5Y_8Mn_4O_{21}$ and $Ba_5Y_7Mn_4O_{19.5}$ compounds by sintering the pellets at 1290 °C for 30 h under an oxygen partial pressure of less than 10^{-6} Pa to avoid oxidization of Mn^{2+} into Mn^{3+} or a higher valence state of Mn ions. The atomic ratios of the Y, Ba, and Mn of the samples were measured using inductively coupled plasma atomic emission spectroscopy (ICP-AES). The compositions of the synthesized samples coincided with the nominal compositions within the error limit of the ICP-AES experiments.

Phase identification of the samples was carried out by X-ray powder diffraction (XRD) using a Rigaku D/max 2500 diffractometer with Cu K_α radiation (45 kV × 250 mA) and a graphite monochrometer. The XRD data for Rietveld refinement were collected in a 2θ range from 5° to 130° with a step size of 0.02° and a sampling time of 1 s per step. The magnetic properties were measured by a superconducting quantum interference device magnetometer (MPMS 7, SQUID). The electric resistivity of well sintered samples was investigated through I–V character measurement by a KEITHLEY 617 Programmable Electrometer in a temperature range of 77 K–300 K. The permittivities of the samples were measured using an NF-2353 LCR-meter with a variable temperature chamber.

3. Experimental results and discussion

3.1. Crystal structure

Single-phase samples with atomic ratios of Ba:Y:Mn = 5:8:4 and 5:7:4 were obtained according to phase identification by XRD. The XRD patterns can be indexed by the space group $I4/m$ and are consistent with those of the $Ba_5RE_8Mn_4O_{21}$ compounds reported in Refs. [4]–[6].

Rietveld refinement of the full XRD patterns was performed using the FullProf program.[7] For the Y7 sample, the isotropic temperature parameter (B) of the O ions is taken from the refined results of Y8. The occupancy factors of the two Y sites, Y(1) and Y(2), in Y7 are given the same starting value of 0.875, and then recalculated during the refinement. Table 1 lists the refined structural parameters for the two samples, Y8 and Y7, at room temperature. Figure 1 shows the observed and calculated XRD patterns, and the difference profiles from Rietveld refinement.

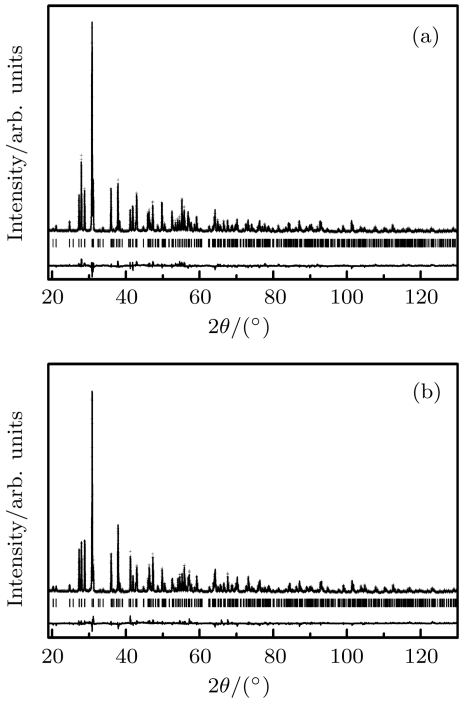


Fig. 1. Observed (cross), calculated (continuous line), and difference (bottom line) XRD profiles for $Ba_5Y_{8-x}Mn_4O_{21-1.5x}$ compounds at room temperature. Panels (a) and (b) are for Y8 and Y7, respectively.

The lattice parameters of the Y7 compound are smaller than those of Y8. This is caused by the lower amount of Y content in Y7 than in Y8. For the Y7 compound, the calculated occupation number of the Y(2) site is less than that of the Y(1) site, indicating that the Y vacancies prefer to occur at the Y(2) site. The change in the $Y(2)O_7$ polyhedra due to the absence of Y in Y7 also implies that the Y(2) site is the preferred site for Y vacancies, which will be discussed below.

In the $Ba_5RE_8Mn_4O_{21}$ structure, the metallic ions arrange in the ab plane, forming layered structures along the c axis at $z = 0$ and $z = 1/2$. The adjacent layers are displaced from each other by moving $1/2(\boldsymbol{a} + \boldsymbol{b})$.

Table 1. Refined structural parameters for the $Ba_5Y_{8-x}Mn_4O_{21-1.5x}$ compounds, Y8 and Y7, at room temperature, 1 Å = 0.1 nm.

	Atom	Site	x	y	z	Occup.	B/Å^2
Sample: Y8	Y1	8h	0.2478(1)	0.1689(1)	0	1	0.33(2)
Symmetry: tetragonal	Y2	8h	0.4124(1)	0.3580(1)	0	1	0.49(3)
Space group: $I4/m$	Ba1	2a	0	0	0	1	0.80(4)
a =13.8539(1)/Å	Ba2	8h	0.5351(1)	0.1398(1)	0	1	0.72(2)
c = 5.7412(1)/Å	Mn	8h	0.0383(2)	0.2482(2)	0	1	0.73(4)
V = 1101.90(2)/Å^3	O1	2b	0	0	0.5	1	1.6(11)
R_p=13.0%	O2	8h	0.6307(6)	0.9626(5)	0	1	1.31(15)
R_{wp}=13.6%	O3	16i	0.6753(5)	0.5458(3)	0.7475(13)	1	0.76(7)
R_{exp}=8.7%	O4	16i	0.3533(4)	0.2473(3)	0.2344(11)	1	0.76(7)
Sample: Y7	Y1	8h	0.2483(1)	0.1692(1)	0	0.90(1)	0.23(2)
Symmetry: tetragonal	Y2	8h	0.4121(1)	0.3590(1)	0	0.85(1)	0.40(3)
Space group: $I4/m$	Ba1	2a	0	0	0	1	1.49(3)
a= 13.8436(1) Å	Ba2	8h	0.5358(1)	0.1403(1)	0	1	1.57(2)
c = 5.7362(1) Å	Mn	8h	0.0392(2)	0.24776(2)	0	1	1.23(4)
V = 1099.32(2) Å^3	O1	2b	0	0	0.5	0.72(1)	1.6
R_p=12.5%	O2	8h	0.6325(5)	0.9569(5)	0	1	1.31
R_{wp}=13.3%	O3	16i	0.6880(4)	0.5487(3)	0.7604(14)	0.93(1)	0.76
R_{exp}=8.6%	O4	16i	0.3534(3)	0.2379 (3)	0.2238(12)	0.93(1)	0.76

Figure 2 shows a schematic representation of one layer of the $Ba_5Y_8Mn_4O_{21}$ structure. The coordination polyhedron of Y ions, YO_7, is a combination of a trigonal prism and a rectangular pyramid. The coordination polyhedron of Mn ions, MnO_5, is a rectangular pyramid. The coordination polyhedron of Ba(1) ions, $Ba(1)O_{10}$, is a dodecahedron with a quadrangular prism capped with two rectangular pyramids on two sides. $Ba(2)O_{10}$ is an irregular tetrakaidecahedron. Four $Y(2)O_7$ polyhedra form a $Y(2)O_7$ unit block with the common apical vertex O(1) and sharing triangular faces. The O(1) is in the centre of the $Y(2)O_7$ unit block, and coordinated with four Y(2) ion (Y(2)–O(1) distances, 2.300 Å for Y7; 2.312 Å for Y8) and two Ba ion (Ba(1)–O(1) distances, 2.868 Å for Y7; and 2.871 Å for Y8). Four Y(2) ions form a square surrounding the O(1) anion, and the edge lengths of the square are 3.252 Å for Y7 and 3.270 Å for Y8. Four $Y(1)O_7$ polyhedra connect the $Y(2)O_7$ unit block by sharing an edge of the $Y(2)O_7$ polyhedron. Table 2 lists the values of the principle metal–oxygen distance d, multiplicity n, and principle bond angles of O–Mn–O for Y8 and Y7.

The Y(2)–O(4) bond lengths in the $Y(2)O_7$ polyhedra of Y8 show a large difference from those in Y7. The distances between Y(2) and O(4) are 2.262 Å in Y7 and 2.198 Å in Y8. The value of 2.198 Å in Y8 is much smaller in comparison with the sum of the ionic sizes of Y^{3+} (r = 0.96 Å, CN = 7) and O^{2-} (1.38 Å, CN = 4).[8,9] As mentioned above, four $Y(2)O_7$ polyhedra

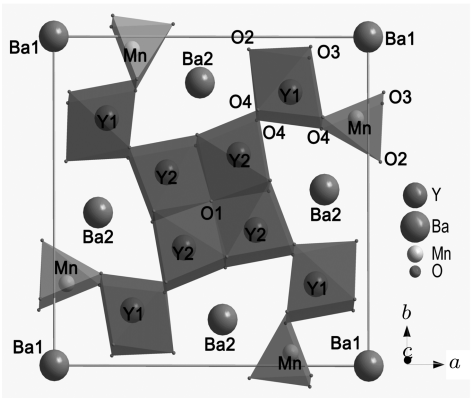


Fig. 2. Schematic representation of one layer of the $Ba_5Y_8Mn_4O_{21}$ structure along the c axis.

form a $Y(2)O_7$ unit block by sharing a triangular face between each other (in Fig. 2), and the distance between two neighboring Y(2) ions is 3.270 Å. However, in the stable Y-oxide of Y_2O_3 ($Ia\bar{3}$ at room temperature), the YO_6 octahedra connect with each other by sharing edges, and the shortest distance between two Y ions is about 3.532 Å. Therefore, there may exist a

Table 2. Values of metal–oxygen distance d (Å), the number of equal metal–oxygen distances (n), and the angles (degree) of O–Mn–O for Y8 and Y7.

Bond		d	n	Bond		d	n
Y8				Y7			
Y1	–O2	2.482	×1	Y1	–O2	2.402	×1
	–O3	2.437	×2		–O3	2.389	×2
	–O4	2.265	×2		–O4	2.161	×2
	–O4	2.373	×2		–O4	2.480	×2
Y2	–O4	2.198	×2	Y2	–O4	2.262	×2
	–O1	2.312	×1		–O1	2.300	×1
	–O3	2.314	×2		–O3	2.333	×2
	–O3	2.393	×2		–O3	2.426	×2
Ba1	–O1	2.871	×2	Ba1	–O1	2.868	×2
	–O3	2.884	×8		–O3	3.076	×8
Ba2	–O2	2.699	×1	Ba2	–O2	2.690	×1
	–O2	2.788	×1		–O2	2.871	×1
	–O2	2.874	×2		–O2	2.872	×2
	–O3	2.947	×2		–O3	2.751	×2
	–O4	3.221	×2		–O4	3.138	×2
	–O4	3.313	×2		–O4	3.217	×2
Mn	–O2	1.980	×1	Mn	–O2	2.012	×1
	–O3	2.097	×2		–O4	2.097	×2
	–O4	2.141	×2		–O3	2.182	×2
O–Mn–O angles (degree)				O–Mn–O angles (degree)			
	O2–Mn–O3	96.5			O2–Mn–O3	89.8	
	O2–Mn–O4	110.3			O2–Mn–O4	108.1	
	O3–Mn–O3	85.3			O3–Mn–O3	90.9	
	O3–Mn–O4	152.4			O4–Mn–O3	161.6	
	O3–Mn–O4	85.5			O4–Mn–O3	85.1	
	O4–Mn–O4	90.8			O4–Mn–O4	93.2	

Note: deviations are 0.009 Å and 0.3 ° for distances and angles, respectively.

repelling force between Y(2) ions in the $Y(2)O_7$ unit block due to the short distance between Y(2) ions. The repelling force pushes Y(2) towards O(4), resulting in the strange short length of the Y(2)–O(4) bond. In the Y7 compound, if the Y vacancies tend to occur at the Y(2) sites as calculated above, the lattice strain in the Y(2) square will be released. The relatively long length of the Y(2)–O(4) bond in the Y7 compound supports the calculated results that the Y vacancies occur preferentially at the Y(2) sites.

3.2. Magnetic property

The temperature-dependent magnetization (M) values of the two samples are measured under a magnetic field of 200 Oe (1 Oe = 79.5775 A/m) in zero-field-cooled (ZFC) and field-cooled (FC) processes, as shown in Fig. 3. The inverse of susceptibility as a function of temperature is shown in the inset of Fig. 3. The Curie constant and Weiss constant obtained through Curie–Weiss fitting of the data are: C (Curie constant) = 16.88 emu · K/(Oe · mol-f.u) where f.u. denotes formula unit, θ (Weiss constant) = –30.19 K for Y8 and C = 16.81 emu · K/(Oe · mol-f.u.), θ = −32.11 K for Y7. The negative Weiss constant indicates that there are antiferromagnetic interactions between the magnetic ions (Mn ions) in the samples. The values of the effective paramagnetic moment (μ_J) of the Mn ion deduced from the Curie constant are 5.81 μ_B per Mn ion in Y8 and 5.80 μ_B per Mn ion in Y7. The obtained value of μ_J is close to the theoretical value of 5.92 μ_B per Mn^{2+}. This indicates that Mn^{2+} ions are the dominant Mn ions in the samples, and that the $Mn^{2+}(3d^5)$ ions take the high-spin configuration due to stronger Hund coupling than the crystal field stabilization energy.

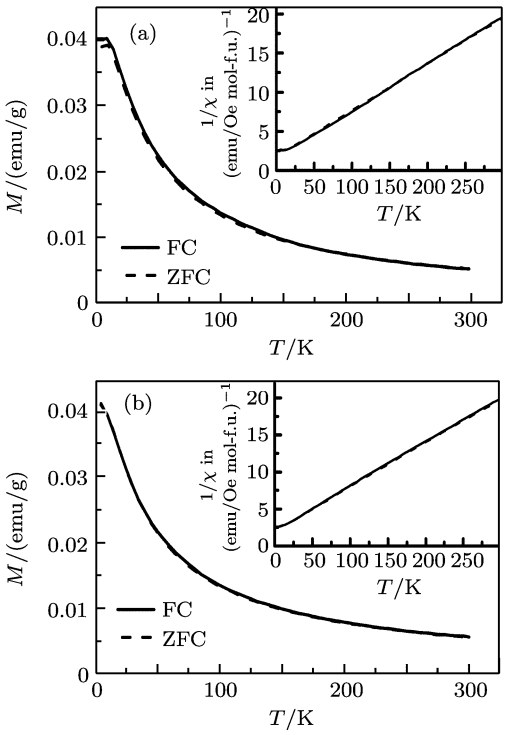


Fig. 3. Magnetizations each as a function of temperature under a magnetic field of 200 Oe in zero-field-cooled (ZFC) and field-cooled (FC) for samples (a) Y8 and (b) Y7.

3.3. Conductive property

The temperature-dependent resistivity (ρ) values of the two samples are measured in a temperature range of 77 K–300 K. Figures 4(a) and 4(b) show the lnρ–1/T plots. The temperature dependence of the resistivity is divided into two main regions: (i) the low-temperature region (77 K–175 K for Y8 and 77 K–170 K for Y7; BC segment) and (ii) the high-temperature region (above $\sim$ 175 K for Y8 and above $\sim$ 170 K for Y7; AB segment). In the low-temperature region, the resistivity slowly increases with decreasing temperature. The resistivity values of Y7 and Y8 at 77 K are $\rho_{\rm Y7} =\sim 1.3\times10^{14}\ \Omega\cdot$mm and $\rho_{\rm Y8} =\sim 2.8\times10^{14}\ \Omega\cdot$mm within the order of magnitude of the characteristic resistivity for insulators. Therefore, the two samples are believed to be in an insulating state in the BC region. In the high-temperature region (AB segment), the resistivities of the two samples rapidly decrease with increasing temperature, and obey the Arrhenius equation:[10] $\rho(T)\propto\exp(E_{\rm a}/kT)$, where $E_{\rm a}$ is the activation energy of the conductive carrier and k is Boltzmann's constant. The slope of the linear ln ρ–1/T plot corresponds to $E_{\rm a}$. The linear variation in ln $\rho(T)$–1/T supports the existence of the thermally activated transport property of the material. Different slopes of lnρ versus 1/T plots in different temperature ranges are observed for both samples in Fig. 4, and the changes in the slope occur at $\sim$ 205 K and $\sim$ 245 K for Y8 and at $\sim$ 240 K for Y7.

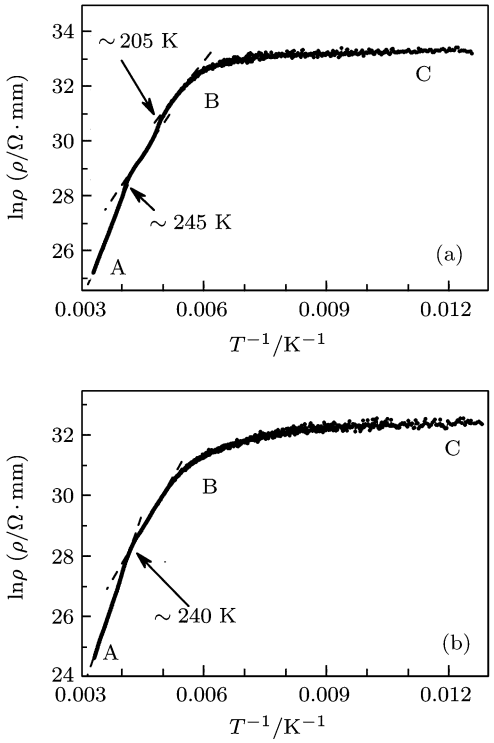


Fig. 4. Variations in lnρ versus 1/T for the samples: (a) Y8 and (b) Y7. The dashed line shows the linear fitting of the data.

The conduction mechanisms may be complex and complicated. In the low-temperature regions (below $\sim$ 175 K for Y8 and $\sim$ 170 K for Y7), the low activation energy suggests the presence of an intrinsic conduction in each of the materials: the density of conductive carriers (electrons and holes) is very low due to the wide energy gap, and the mobility of carriers increases slightly with increasing temperature. Meanwhile, lattice scattering plays an important role in the electrical resistance mechanism.[11] The materials are each in the insulating state. However, as the temperature increases beyond $\sim$ 175 K for Y8 and above $\sim$ 170 K for Y7, some conduction elements are thermally activated, such as thermal excitations of the ion vacancies ($V_{\rm O}$ and $V_{\rm Y}$), which act as dopants or ionic carriers, the hopping of electrons between Mn^{2+} and Mn^{3+}, which may exist due to the presence of ion vacancies, and grain boundary conduction. The changes in the slopes of the lnρ–1/T plots indicate that multiple conduction processes exist in the materials with different activation energies. The activation energy $E_{\rm a}$ values obtained by linear fitting of the data are 0.20 eV (175 K–240 K) and 0.34 eV (240 K–300 K)

for Y7, 0.18 eV (180 K–205 K), 0.20 eV (205K–245 K), and 0.33 eV (245 K–300 K) for Y8. The resistivities at 300 K are $\rho_{Y7} = 5.07 \times 10^{10}\ \Omega \cdot$mm for Y7, $\rho_{Y8} = 9.65 \times 10^{10}\ \Omega \cdot$mm for Y8, which are within the order of magnitude of the characteristic resistivity for semiconductors. The insulator–semiconductor transitions occur around 175 K for Y8 and 170 K for Y7. The resistivity of Y8 is larger than that of Y7 at the same temperature, which may be caused by the lower ion vacancies in Y8 than in Y7.

3.4. Dielectric property

The temperature-dependent dielectric constant is measured in a temperature range of 80 K–300 K under different frequencies. Figure 5 shows the temperature dependences of the dielectric constants of Y8 and Y7, where ε'_r and ε''_r represent the real and imaginary parts of the dielectric constant, respectively. The dielectric constant is almost independent of temperature below $\sim$ 175 K, while it quickly increases with increasing temperature up to above $\sim$ 175 K, which is consistent with the observation of the insulator–semiconductor transition by direct current resistivity measurements.

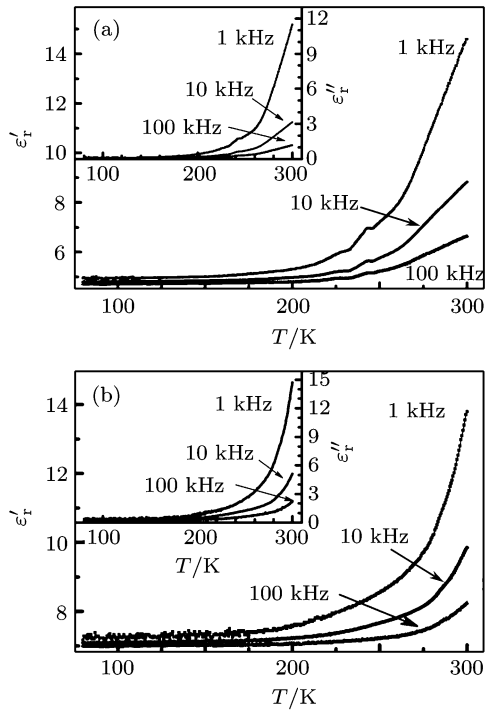


Fig. 5. The temperature dependences of the dielectric constants of the samples: (a) Y8, (b) Y7. The insets show the imaginary part of the dielectric constant.

At temperatures above $\sim$ 175 K, the dielectric constants show strong frequency dispersion, suggesting that mobile charge carriers (such as charged vacancies and ions) might be the origin of the leakage current in this temperature range according to Jonscher.[12] A dielectric anomaly is observed around 240 K in Y8, in concert with the resistivity anomaly of Y8, which indicates the thermal activation of a conduction element at this temperature.

4. Conclusion

In this work, $Ba_5Y_{8-x}Mn_4O_{21-1.5x}$ solid solution compounds are prepared with atomic ratios of Ba:Y:Mn = 5:8:4 ($x = 0$) and 5:7:4 ($x = 1$) by an atmosphere-controlled solid-state reaction technique. XRD analysis shows that the $Ba_5Y_{8-x}Mn_4O_{21-1.5x}$ compound is a Y-deficient solid solution and has a tetragonal structure with space group $I4/m$. The Rietveld refinement results reveal that the vacancies of Y occur preferentially at the Y(2) site in the Y7 sample. Magnetic measurements indicate that antiferromagnetic interactions exist between the Mn ions in the compounds. The calculations of the values of the effective paramagnetic moment (μ_J) of the Mn ions indicate that Mn^{2+} ions are the dominant ions in the samples. The temperature-dependent resistivity measurements show that insulator–semiconductor transitions appear at about 170 K for Y7 and 175 K for Y8. The variations in dielectric constants versus temperature are consistent with those of resistivity in the two samples.

References

[1] Rao C N R and Raveau B 1998 *Colossal Magnetoresistance, Charge Ordering and Related Properties of Manganese Oxides* (Singapore: World Scientific)
[2] Narlikar A V (ed.) 2005 *Frontiers in Magnetic Materials* (Berlin: Springer)
[3] Fiebig M 2005 *J. Phys.* D: *Appl. Phys.* **38** R123
[4] Muller-Buschbaum H K and Kluver E 1992 *Z. Anorg. Allg. Chem.* **612** 21
[5] Muller-Buschbaum H K and Rabbow CH 1992 *J. Alloys Compd.* **190** L27
[6] Kluver E, Peters E and Muller-Buschbaum H K 1992 *J. Alloys Compd.* **189** 101
[7] Rodriguez-Carvajal J 1993 *Physica* B **192** 55
[8] Shannon R D and Prewitt C T 1969 *Acta Cryst.* B **25** 925
[9] Shannonn R D 1976 *Acta Cryst.* A **32** 751
[10] Arrhenius S 1889 *Z. Phys. Chem.* **4** 226
[11] Bardeen J and Shockley W 1950 *Phys. Rev.* **80** 72
[12] Jonscher A K 1983 *Thin Solid Films* **100** 329